Eur. Phys. J. D (2005)
DOI: 10.1140/epjd/e2005-00222-6

THE EUROPEAN PHYSICAL JOURNAL D

Single molecule vibrationally mediated chemistry

Towards state-specific strategies for molecular handling*

J.I. Pascual[a]

Institut für Experimentalphysik, Freie Universität Berlin Arnimallee 14, 14195 Berlin, Germany

Received 4 April 2005 / Received in final form 26 May 2005
Published online 9 August 2005 –

Abstract. Tunnelling electrons may scatter inelastically with an adsorbate, releasing part of their energy through the excitation of molecular vibrations. The resolution of inelastic processes with a low temperature scanning tunnelling microscope (STM) provides a valuable tool to chemically characterize single adsorbates and their adsorption mechanisms. Here, we present a molecular scale picture of single molecule vibrational chemistry, as resolved by STM. To understand the way a reaction proceed it is needed knowledge about both the excitation and damping of a molecular vibration. The excitation is mediated by the specific coupling between electronic molecular resonances present at the Fermi level and vibrational states of the adsorbate. Thus, the two-dimensional mapping of the inelastic signal with an STM provides the spatial distribution of the adsorbate electronic states (near the Fermi level) which are predominantly coupled to the particular vibrational mode observed. The damping of the vibration follows a competition between different mechanisms, mediated via the creation of electron-hole pairs or via anharmonic coupling between vibrational states. This latter case give rise to effective energy transfer mechanisms which eventually may focus vibrational energy in a specific reaction coordinate. In this single-molecule work-bench, STM provides alternative tools to understand reactivity in the limit of low excitation rate, which demonstrate the existence of state-specific excitation strategies which may lead to selectivity in the product of a reaction.

PACS. 68.37.Ef Scanning tunneling microscopy (including chemistry induced with STM) – 68.43.-h Chemisorption/physisorption: adsorbates on surfaces – 63.22.+m Phonons or vibrational states in low-dimensional structures and nanoscale materials

1 Introduction

The investigation of reactions employing electrons or photons as excitation source has provided important knowledge about the dynamics of chemical transformations [1,2]. These methods explore new routes of chemical processing and catalysis, as alternative to empirical approaches in which industry has been based during the last centuries. One of the main consequences of this advance is the possibility of influencing the course of a reaction [3]. Control of the particle energy, flux, and coherence allows the exploration of alternative reaction pathways and products as those that would be obtained by thermal chemistry. The objective behind the purely fundamental understanding is the control of the course of a reaction by proper adjustment of the excitation source.

In a thermally induced reaction of, for example, a molecule adsorbed on a surface the thermal energy is distributed among all vibrational degrees of freedom of the adsorbate/surface system. Molecular vibrational excited states are populated following a Maxwell-Boltzman statistics. The thermodynamical equilibrium lasts for times much larger than the characteristic time-scale of a molecular vibration. Therefore, time is not (generally) an issue in a thermal reaction. In these circumstances, the reaction will take place along those coordinates having the lowest activation barrier.

Photochemistry and electron induced chemistry have developed several strategies for actuating on a reaction [3–5]. The reaction mechanism is very sensitive to the time scale of the excitation process relative to excitation lifetime. Laser femtosecond pulses provide a time-resolved picture of the excitation dynamics. On metals, a short (few femtoseconds) pulse induces a non-adiabatic excitation of hot-electrons at the surface, which equilibrates to a (hot) Fermi-Dirac distribution in the time scale of a picosecond. The hot electron sea cools down by exciting phonons in a time scale of several picoseconds [6]. Scattering of hot electrons with electronic states of an adsorbate may induced a reaction. In some cases, reactions are mediated by the adsorbate populating ionic

* The author acknowledges his co-workers in the work presented here, H. Conrad, N. Lorente, H.-P. Rust, and Z. Song, as well as collaborations with J. Gómez Herrero, J.J. Jackiw, D. Sánchez-Portal and P.S. Weiss.

[a] e-mail: pascual@physik.fu-berlin.de

transition states. On chemisorption systems, the lifetime of electronic excitations is usually very short, but reactions can still take place in the electronic ground state when the adsorbate becomes highly vibrationally excited. Due to the high power density employed in femtosecond photochemistry, the excitation rate is generally larger than vibrational damping rates (in metal surface this is in the picosecond time scale due mainly to relaxation into electron-hole pair excitations). Therefore, a DIMET (desorption induced by multiple electronic transitions) scheme dominates the reaction [7]. The fast excitation scheme thus results in thermal-like mechanism of reaction, lasting for times in the order of the duration of the hot electron sea thermodynamical equilibrium. For thermal-like reactions selective strategies have been developed based in the *selective* vibrational preparation of molecules with IR pulses [8,9].

When the excitation rate is lower than the vibrational damping rate, multiple excitation schemes become more inefficient. In this case the reaction takes place if a single excitation provides sufficient energy to the reaction coordinate for climbing the activation barrier in a coherent one-step process — the so-called DIET (desorption induced by electronic transitions) scheme. When several possible pathways compete, the low excitation rate favors those schemes employing a smaller number of excitations. In a single excitation process, the reaction rate is linear with the excitation rate. Since the vibrational energy is not spread along different coordinates in a thermal like fashion the outcome of the reaction may differ from those found in DIMET, thus easing selectivity [10].

One can also actuate on the course of a reaction by selecting the method of placing energy into the adsorbate. In mode-specific strategies energy is placed directly on a vibrational state. The selective excitation of specific vibrations was demonstrated few decades ago, by resonantly coupling a laser with vibrational modes [11,12]. Here, one specific vibrational coordinates is directly excited without the participation of electronic excitations; thus, energy re-distribution processes are less efficient. A nice example which is relevant for the results presented here is the IR induced desorption of NH_3 [13,14]. Resonant coupling of IR photon with the ν_s(N–H) mode ($E(\nu_s(\text{N–H}) \sim 420$ meV) produce NH_3 desorption following a double excitation mechanism. In case of fast energy spread processes dominate two single excitation would no suffice to induce the cleavage of the ∼600 meV chemisorption bond. Instead, the authors propose that the external vibrational coordinate (the molecule-surface stretching coordinate) store the energy of the two consecutive ν_s(N–H) fundamental excitation. In these works the concept of energy localization in the reaction coordinate was introduce as the alternative to fast energy spread mechanisms characteristic of thermal like (vibrational heating) processes [15]. The cost of these mode-specific strategies is a lower efficiency.

In the last years, scanning tunnelling microscopy (STM) has been employed for the manipulation of single atoms and molecules. In the first approaches model nanostructures were constructed by the so-called *lateral manipulation* [16–20]; atoms and molecules were dragged or pulled along the surface by the STM tip [21].

The STM has also evolved as a tool for inducing different types of chemical transformations on single adsorbates by means of the tunnelling electron current. Tunnelling electrons interacting inelastically with an adsorbate located at the tunnel junction may excite either vibrational or electronic states. In general, inelastic electrons represent a small fraction (f_i) of the tunnelling current (I_t). These local excitations can induce an effect on a single adsorbate *with the STM tip playing no role*. In most of the cases, the transformation consists in the cleavage of a molecular bond (internal or external). Key experiments during the past years have demonstrated that chemistry at the single-molecule scale provides complementary information to classical surface chemistry techniques for the investigation of reaction dynamics producing either molecular dissociation [22–26], or molecular motion (desorption, rotation, translation) [27–33] when specific vibrational states of the adsorbate are excited. On several of these experiments [28–32], the effect of the excitation of an internal bond was the inducement of molecular motion, i.e. the rupture of the adsorption bond, revealing the operation of effective mechanisms of vibrational energy transfer through internal vibrational pathways [34].

The experimental parameters that allow the induction and control of a reaction are the tunnelling electron energy (eV_s, where V_s is the applied sample bias) and current (I_t). The first one select the excitation by tuning the electron energy; the second controls the excitation rate. Typically an STM applies power intensity in the rage of 1 nW/nm^2 (for example 1 nA and 1 V). For 1 nA of tunnelling current, the time elapsed between tunnelling electrons is ∼160 ps, and this charge transfer rate can be tuned typically in a window of 4 orders of magnitude around this point. In this way, by controlling the excitation rate [7] it is possible to induce both reactions mediated by vibrational heating of the adsorbate [27,35], when the tunnelling timescale approaches that of vibrational excitations (typically reached for tunnelling currents above a few tens of nA's), or reactions following a DIET scheme [28].

A second characteristic of chemistry induced by an STM concerns the excitation mechanism. The energy of the tunnelling electron is donated to the adsorbate through the scattering with molecular states. In a molecule/metal chemisorption system, the surface and molecular states are strongly coupled, causing tunnelling transitions typically faster than nuclear motions. Fast ionic transition states do not favor the energy redistribution processes [36]. Thus, it is possible to find that one specific vibration can be excited simply by adjusting the sample bias voltage above to its frequency. The result is similar to resonantly coupling IR lasers with vibrations [11,12] with just one exception: in STM the energy of the tunnelling electrons is distributed in window defined by the electrochemical potential of tip and sample (see Fig. 1). Thus, by selecting a fundamental mode frequency STM can excite also higher vibrational overtones which may

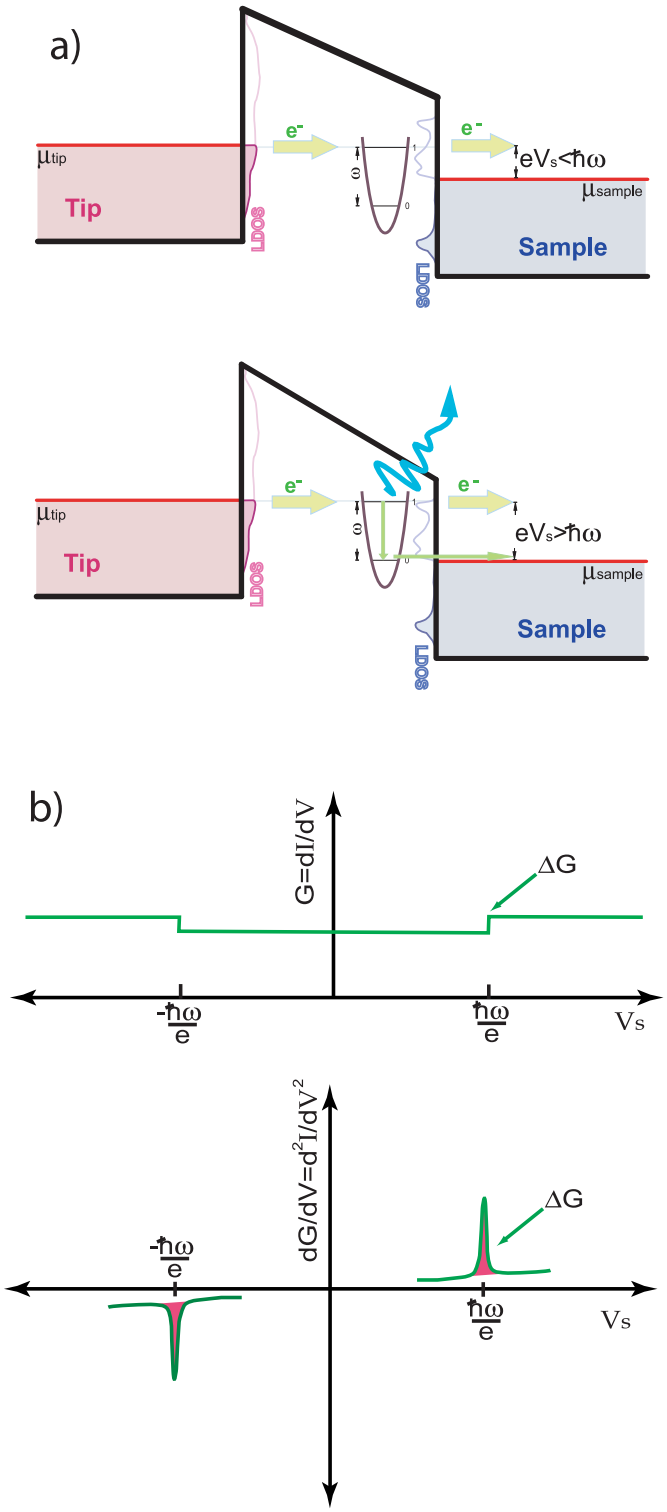

Fig. 1. (a) Model potential energy diagram of a tunnelling junction with an adsorbed molecule in it. The vibrational degrees of freedom of the adsorbate are included as a simple harmonic potential. Only when the final state becomes accessible to the tunnelling electrons (i.e. when it corresponds to unoccupied states of the surface) the inelastic channel is open. (b) The effect of the inelastic channels is ideally a slight stepwise increase in the tunnelling conductance, and correspondingly, a peak in a d^2I/dV_s^2 vs. V_s plot.

have lower frequency due to anharmonicities of the potential. On the contrary, the photon energy of a IR laser is fixed to match resonantly the energy of a specific vibrational transition, usually the fundamental excitation. As we shall see later, both techniques have obtained similar results with a model problem, the desorption of NH_3 from a Cu(100) surface [13,14,31].

Tunnelling electron induced processes have a valuable fundamental significance, because the single molecule approach leads to complementary information respect to that obtained by photochemistry. Tunnelling electrons can induce reactions in similar regimes, and with similar excitation mechanisms as other techniques, but STM chemistry explore reactions having very little efficiency, due to its high sensitivity. STM can also detect transition through reaction pathways along the surface (diffusion, dissociation, rotation and conformational changes) which are not so directly accessible to other techniques.

In this article, we review our latest results on the topic of vibrationally mediated molecular transformations with the purpose of drawing a molecular-scale picture of how a reaction proceeds. We restrict the description to vibrational-mediated processes. Electronic excitations can also be used for inducing single molecule transformation, but the reaction pathway might differ from those presented here [25,26,33].

The first part deals with the excitation of molecular vibrations, which can be studied applying scanning tunnelling spectroscopy (STS) techniques. We will present measurements on some model systems which illustrate the role of molecular resonances in the inelastic scattering. Besides, the investigation of inelastic processes revealed valuable information about several elementary processes like intramolecular energy transfer via inter-mode coupling [28,30,31], conformational changes [38–40] or fundamental pathways of chemical reactions [22–24,31]. In the second part, we describe some of these vibrational damping processes, which eventually lead to reaction. Using a very well studied model system, ammonia on Cu(100), we will describe several of the possible processes that might take place when tunnelling electrons are used to excite a molecular vibration. In this case, we find that a it is possible to design a mode-specific strategy for controlling the motion of a single molecule [31,37].

2 Mechanism of vibrational excitation by tunnelling electrons

Soon after the discovery of STM, Binnig, García and Rohrer [41] proposed a strategy to obtain the vibrational structure of a single molecule based on a technique called Inelastic Electron Tunnelling Spectroscopy (IETS) [43]. IETS was first developed in 1966 by Jacklevic and Lambe [44], who observed that tunnelling electrons were able to excite vibrational modes of a thin molecular layer buried between two metallic electrodes and an oxide layer (i.e. a tunnelling barrier). The vibrational excitation occurs when the tunnelling electron energy match that of

a vibrational eigenmode. Upon activation of these inelastic scattering processes an additional transport channel is open, inducing a slight increase of the conductivity of the tunnel junction. From the detection of energy thresholds for vibrational excitation one could resolve the vibrational structure of the buried molecular layer.

The configuration of a STM junction is similar when the oxide layer is substituted by the tip-sample vacuum gap. The advantages are that molecules are adsorbed on an atomically clean metal surface with a well-defined geometry. The adsorption geometry and orientation of the adsorbate can be well-known. The effect of the STM tip or the high electric field is in general negligible. STM works under the same controlled conditions as other classical surface chemistry techniques, but with a large improvement regarding the spatial resolution of the adsorbate's vibrational structure.

However, there are important differences between inelastic electron tunnelling spectroscopy with STM (IETS-STM) and traditional IETS, related to the nature of the excitation mechanism. In the STM configuration, the majority of the electron current tunnels though the adsorbate itself, therefore having a strong component of molecular derived resonances [45]. This results in local inelastic scattering mechanisms strongly mediated by the electronic configuration of the molecule/surface complex. In IETS, however, the tunnelling current is less focused on the adsorbate. Therefore, the excitation follows predominantly a non-local mechanism as, for example, dipolar interaction between electron and molecule [42].

2.1 Working principle

Single-molecule vibrational spectroscopy identifies the energy of a molecular vibration by detecting small changes in the conductivity of the tunnelling junction due to onset of inelastic scattering processes. The tip of an STM is placed on top of a molecule and the voltage is ramped. When the electron energy matches a quantum of vibration, the conductance changes abruptly: the STM has detected the mode frequency of an adsorbed molecule (Fig. 1a).

The resolution of inelastic effects depends on two fundamental mechanisms: excitation and detection. They are not equivalent, and both have to be treated for understanding the origin of active modes in the vibrational spectra [46]. The excitation is based on inelastic scattering processes, thus connecting initial and final states with different energy. The inelastic cross-section defines the fraction of tunnelling current through the inelastic channel (f_i). The inelastic fraction is intrinsically connected with the nature and alignment of molecular resonances respect the Fermi level of the molecule/surface system. Therefore, it is very sensitive to the nature of the interaction between between adsorbate and surface.

The detection relies on the effect of the new (inelastic) channel on experimentally observable magnitudes, i.e. the junction differential conductivity ($G = dI/dV_s$). The inelastic channel transports charge in parallel to the elastic scattering channel (i.e. to the channel where initial and final electronic states have equal energy). Hence, as a first approximation, the effect of the vibrational excitations will be a slight increment of the junction conductivity $\Delta G \sim f_i \times G$.

In practice, the inelastic fraction is a number typically smaller than 0.1, corresponding to a change of the total conductance of less than 10%. This change can be detected only under extreme conditions of mechanical stability and energy resolution. To help with the detection of such small signal, the second derivative of the tunnelling current ($d^2I/dV_s^2 = dG/dV$) is usually measured. This magnitude show peaked features at energies corresponding to the opening of an inelastic channel (Fig. 1b). Since the inelastic channel can be opened indistinguishably by tunnelling electrons travelling from every electrode peaks appear at the same bias values, independently of the sample polarity.

To detect the weak d^2I/dV_s^2 signal lock-in techniques are usually employed. Due to the low signal, acquiring vibrational spectra requires large acquisition time. Usually, the measurement of one spectrum takes from tens of seconds to minutes. Such stability can be only reached when working at very low temperatures, as for example, when the STM head in thermal equilibrium with a liquid helium reservoir. Working at low temperatures is also an imposed requirement for reaching the appropriate energy resolution to resolve the narrow lineshape of the vibrational peaks. References [47,48] provide a detailed description of experimental issues.

2.2 Experimental results

The first successful detection of a vibrational mode using a STM was the C–H stretch mode of acetylene adsorbed on Cu(100) [49]. Since then, C–H stretch has been detected with more or less intensity in several hydrocarbons by the group of Ho (as reviewed in Ref. [50]) and by the group of Kawai [24,51].

Figure 2 reproduces typical vibrational spectra of three different adsorbate systems, which summarizes the advantages and limitations of this vibrational spectroscopy. One the one hand, IETS-STM can resolve internal vibrations, as it is the case of the C–H stretch mode of acetylene (Fig. 2a), external (hindered) vibrations, as for example the external modes of CO on Cu(110) (Fig. 2b), and even collective modes, as illustrated by the breathing mode of an icosahedral fullerene cavity shown in Figure 2c. In every case, the signal can be resolve in space with sub-nanometre resolution, and in energy with meV resolution. However, the spectra show only a small number of active modes out of all vibrational degrees of freedom.

Thus, a major drawback of IETS-STM is the lack of sensitivity for many of the molecular modes of a molecular-surface system, which remain either inactive or undetected. There is no relation with excitation selection rules from other vibrational spectroscopies like IR, Raman, or EELS. The initial results of IETS-STM point to the fact that active modes depend on the symmetry and configuration of the adsorption geometry. Although

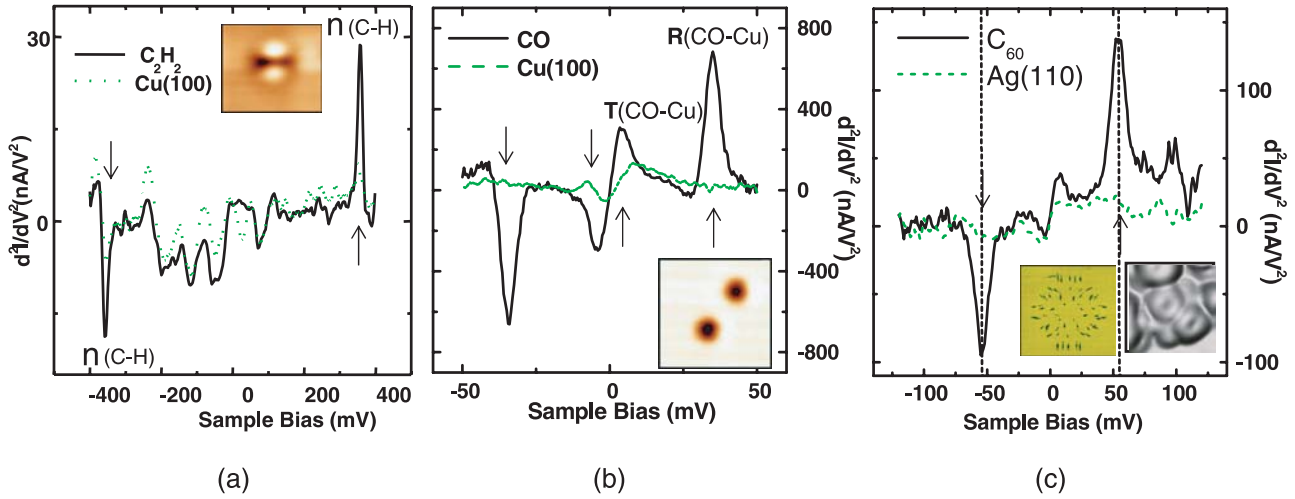

Fig. 2. Vibrational spectra of three different molecular adsorbates. (a) C_2H_2 on Cu(100): peaks at ±356 mV is due to excitation of the C–H stretch vibration. (b) External vibrations of CO on Cu(100): peaks at ±5 mV and ±35 mV are due to excitation of the CO frustrated rotation (R(CO–Cu)) and translation (T(CO–Cu)) respect the Cu(100) surface. (c) C_{60} on Ag(110): peaks at ±55 mV are associated with a breathing mode of the fullerene cavity ($H_u(2)$ mode, shown in the inset). The insets also show the corresponding molecular structure in the STM topography.

the exact origin of selection rules for excitation and detection is unknown, there is general agreement that it must be related to the resonant character of tunnelling transport, first proposed by Persson and Baratoff [45]. For understanding the excitation processes the nature of the molecular chemisorption has to be precisely known. A strong combination of experimental measurements and theoretical simulations must be used in order to understand the fundamentals of IETS-STM.

In this section, we present two different studies on IETS-STM. In both cases, the results are interpreted based on electronic scattering by molecular resonances.

2.3 C_{60} on Ag(110)

A possible experimental approach for demonstrating the resonant character of vibrational excitation is based on the spatial mapping of vibrational signal with sub-molecular resolution, comparing it with the shape of electronic resonances at the Fermi level [52]. A model system for this investigation is C_{60} because of its cage structure with icosahedral (I_h) symmetry. The high symmetry of its atomic structure causes high degeneration of both electronic and vibrational states. In addition, the rigid three-dimensional cage remains highly unperturbed upon adsorption: when C_{60} is adsorbed on a surface the structure of the free-molecule orbitals remains fairly unaltered [53]. On noble metal surfaces, fullerenes behave as electrophilic species; their interaction with the substrate is usually described by a predominantly ionic charge transfer to unoccupied, LUMO derived states. We study here fullerene molecules deposited on a highly anisotropic surface, Ag(110). The deposition was done with the sample at room temperature, while the measurements where performed after cooling down to 5 K.

Figure 3 compares of the electronic configuration of C_{60} on Ag(110) resolved by STS with photoemission and inverse photoemission results. The former is measured on a single molecule forming part of a small island. The junction conductivity dI/dV resembles the (energy-resolved) density of states of the molecule/surface complex. The peaks thus are identified with the position of molecular induced states respect to the Fermi level. The photoemission data is measured on both submonolayer and multilayer regimes. Besides the high spatial resolution, STS reveal more information in the region of unoccupied states, where the spectroscopy is more sensitive to the electronic structure of the surface electrode.

The position of the HOMO- and LUMO-derived resonances coincides in both measurements, giving a HOMO-LUMO gap of 2.3 eV. The electrophilic behaviour of the fullerene molecule causes a closer alignment of the LUMO resonance with the Fermi energy level, as a consequence of the partial filling of the molecules' empty states. Because of this, a small tail of the unoccupied resonance crosses the Fermi energy (Fig. 3b). These states mediate the electron transport for energies around the Fermi level.

STM has proven its ability to resolve the molecular orientation [53,55] and its electronic configuration [56] at the single molecular level, relating it with fundamental aspects of the local molecular adsorption properties [57] such as adsorption site, coordination, symmetry/orientation, and intermolecular interactions. Figure 4a shows a C_{60} island on Ag(110). In contrast with the case of post-deposition annealing, where a $c(2 \times 4)$ molecular superstructure arises [58], here the island does not present a clear ordered structure. The intra-molecular structure also reveals that molecules within the island show different orientations. Figures 4b and 4c show a zoom on two of these molecules, whose internal structure presents one of the symmetries of the icosahedral cage. We associate these

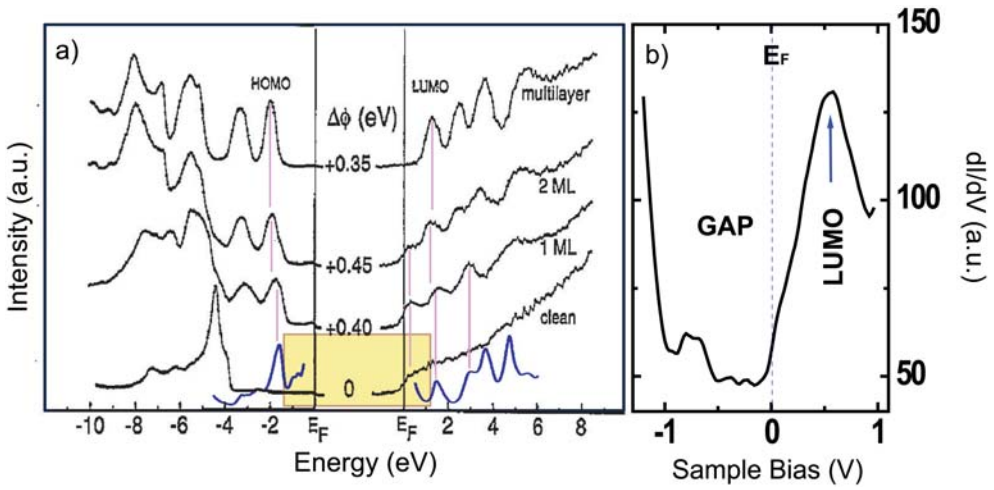

Fig. 3. (a) Comparison of electronic structure of C_{60} on Ag(110) measured by STS, on a single molecule forming part of a domain, and by photoemission and inverse photoemission, for different coverage values. The later is reprinted with permission from reference [54]. The yellow square locates the energy range of the zoomed data, shown in (b). There, the dI/dV vs. V_s plot is shown for electron energies around the substrate Fermi level: the LUMO and gap features indicated in the figure are derived from the C_{60} molecular orbitals after their interaction with the surface.

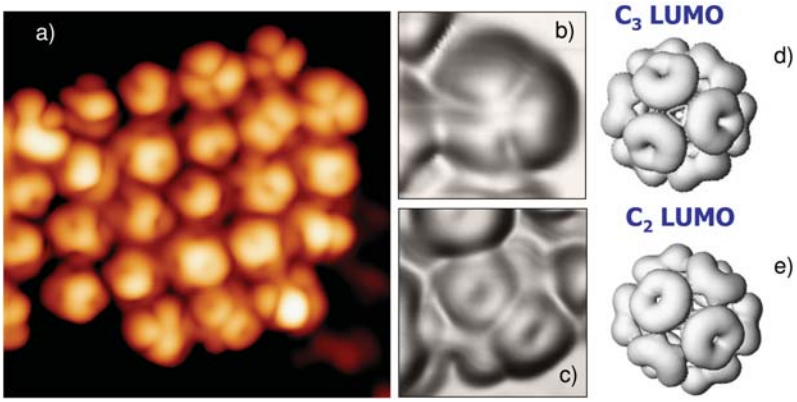

Fig. 4. (a) STM image of a C_{60} island on Ag(110). The intramolecular structure reveals the adsorption of multiple molecular orientations. Only a small number of molecules have intramolecular structure resembling some of the symmetries of the C_{60} cage. In (b) and (c) a zoom of two of these orientations is compared with constant charge isosurfaces of the LUMO orbitals, as view from the (d) three-fold and (e) two-fold symmetry axis. The calculations are done for a free molecule using density functional theory implemented with the SIESTA code [59,60].

structures with molecules having one of their symmetry axis perpendicular to the surface, and therefore probably keeping some degree of degeneracy in their electronic and vibrational states upon adsorption.

It is interesting to compare the internal structure of molecules in Figure 4b with calculations of the spatial shape of their molecular orbitals. Since the perturbation of the C_{60} molecule at the surface is small, this comparison can be done successfully by simply calculating the charge density $\rho(\mathbf{r})$ for the free molecule. Constant $\rho(\mathbf{r})$ surfaces simulate what the STM sees in those cases in which interference between multiple molecular resonances does not play a role [53]. The calculated constant charge isosurfaces for the LUMO orbital of a free C_{60} molecule are shown for comparison in Figures 4d and 4e. The calculations reproduce a structure formed by rings of charge centered at the pentagons of the icosahedral cage. When plotted as seen along the S_2 and S_3 symmetry axis, the LUMO isosurfaces resemble the intramolecular of the STM images. Agreeing with the electronic configuration revealed by the spectra of Figure 3, the calculations demonstrate that electron tunnelling through the molecule is essentially dominated by LUMO-derived states. For this system it is improbable that HOMO states present any significant contribution to the excitation mechanism.

The vibrational structure of a free C_{60} molecule consists on 46 distinct excitations with energy ranging between 33 and 195 meV, which account for the 174 internal vibrations of a molecular cage with icosahedral symmetry. Figure 5a shows the characteristic d^2I/dV_s^2 spectra measured on top of a C_{60} molecule. A narrow peak at a bias value of 54 mV appears at both polarities. The peak is probably associated to the H_g mode corresponding to a gerade breathing of the molecular cage with a larger radial component along the C_{5v} symmetry axis [61]. In the free molecule, this mode is 5-fold degenerate. At the surface, it is expected that the degree of degeneracy changes depending on the specific orientation of the molecule.

The resonant character of the excitation mechanism can be demonstrated by analyzing the spatial distribution of the inelastic signal within the molecular cage. This measurement is done by tuning the sample bias to the value of the inelastic peak, and performing a slow STM image while plotting the d^2I/dV_s^2 signal. This microscopy

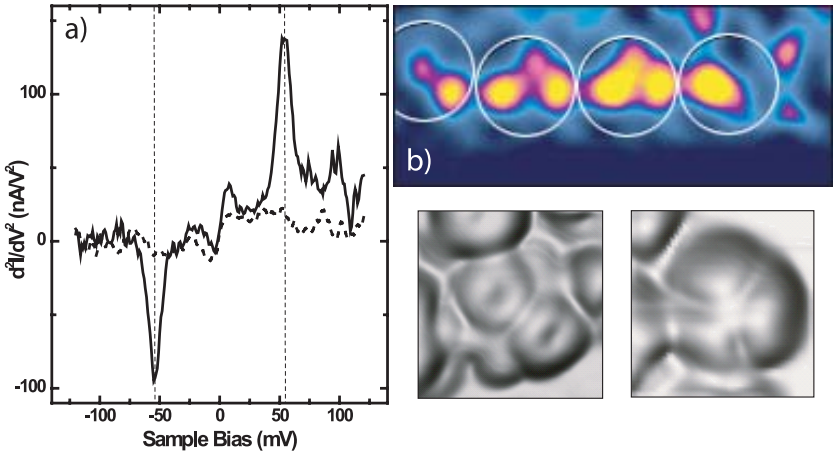

Fig. 5. (a) d^2I/dV_s^2 vs. V_s spectrum of an adsorbed fullerene. The spectrum is compared with that measured on the nearby bare Ag(110) surface. The peaks at ±54 mV correspond to a normalized change in conductance ($\Delta G/G$) of ∼9%. (I = 1.6 nA, V_s = 0.1 V, V_{ac} = 5 mV rms at f_{ac} = 341 Hz). (b) d^2I/dV_s^2 maps on part of a C_{60} island measured at 56 mV. A critical enhancement of the signal is observed on some small locations within the molecular cage. White circles help to locate the position of the molecules in the corresponding topography image (I = 1.6 nA, V_{ac} = 6 mV rms at f_{ac} = 941 Hz). The inelastic maps compare with the shape of LUMO orbitals (below shown STM images for comparison).

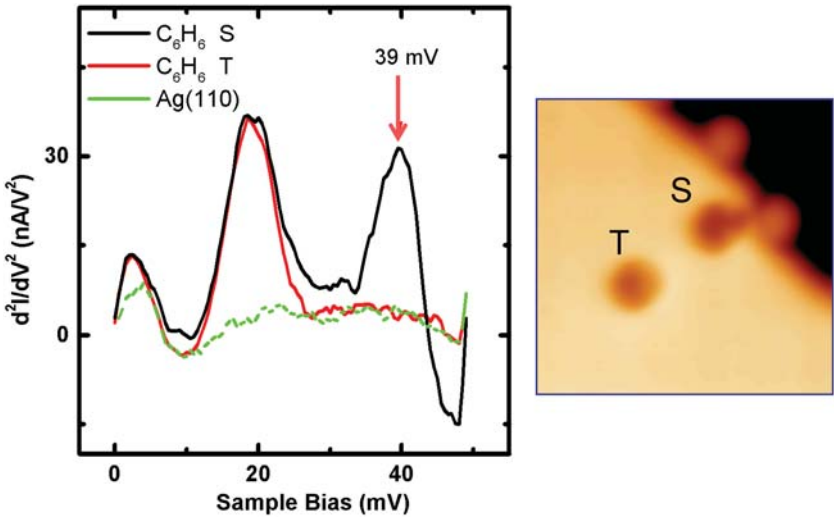

Fig. 6. d^2I/dV_s^2 vs. V_s spectra of adsorbed benzene molecules. For the shake of clarity, the spectra show only the positive bias region. The plot compares a spectrum of a flat-lying molecule on the terrace, marked "T" in the STM image, with that of a molecule close to a kink site ("S" in the image). The proximity of a step disrupts the molecular feature as seen in the STM image, presumably corresponding to a slight tilting of the molecular plane. For this distorted molecule, an additional peak indicated in the figure with an arrow is found I = 2 nA, V_s = 0.1 V, V_{ac} = 4 mV rms at f_{ac} = 641 Hz.

approach is quite powerful for the localization of the inelastic signal within the molecular cage. Here, it can be used to understand the origin of excitation by comparing it with the topography images of Figure 4.

Figure 5b shows a map of the inelastic signal acquired with *dc* sample bias of 56 mV. The inelastic signal has a maximum excitation only at specific locations within the fullerene cavity. Such positions are on most of the molecules randomly distributed within the molecular cage, in consistency with the multiple orientations that the molecule may adopt at the surface. A few amount the molecules show lobes of maximum inelastic signal distributed following some of the symmetries of the fullerene cavity. In particular, the arrangement of the lobes fits with the location of the molecular pentagons. The association of these inelastic maps with the shape of the LUMO shown in Figure 4 reveals the active role of this resonance in the excitation process. The reason why the H_g mode shows the largest signal must be related to the specific vibronic coupling between these two states. Other modes are occasionally detected in the spectra, although their signal lays close to the background. We believe that all the excitation is dominated by the LUMO resonance, since it is the one present at the Fermi level. The occupied molecular states lie below a energy gap, thus having probably a negligible weight at E_F. For smaller systems, the molecular structure is usually further more perturbed upon chemisorption, and the molecular resonances considerably wider. In this case, as we shall see in next section, it is possible to have competition in the excitation mediated by several resonances.

2.4 C_6H_6 on Ag(110)

A smaller molecular system, benzene (C_6H_6), on Ag(110) was also employed to investigate the role of the molecular orientation on the excitation of vibrations. Depending on the sample temperature during deposition benzene molecules populate two different adsorption states with very different properties [62,63]. The weakest state (diffuses easily by the presence of the tip — presumably physisorbed) appears when dosing molecules at sample temperature below 20 K. This is characteristic of a transient adsorption state, trapped at such low temperature by an activation barrier for chemisorption. Dosing above 20 K, the molecules show a very different shape in the STM images (see Fig. 6) and their stability is much larger. In this

case, the molecules populate a chemisorption state probably involving charge donation and back-donation from molecular π states.

Inelastic spectroscopy resolves some of the external vibrational modes associated with every adsorption state [62,63]. Since each state represents a different interaction with the metal surface, their vibrational fingerprint will differ. For the chemisorbed state, inelastic spectra show peaks at ± 4 and ± 19 meV, which were tentatively identified as due to hindered translational and rotational degrees of freedom. For the physisorbed state, two vibrational modes, with energy of 7 meV and 43 meV were also detected. Energy shifts of the modes' energy can not simply account for the large difference between the spectra. The 43 meV mode in the physisorbed case is probably associated with an internal ring bending mode, which is not seen in the case of the chemisorbed one. So, in every case the spectra show different active modes rather than mode-energy shifts. This exemplifies the difficulty in constructing a set of general selection rules, since different minima in the adsorption potential surface may show modes of a different nature in the spectra.

For the molecules lying flat on the surface no other vibration could be detected. However, a local distortion of the adsorption geometry may lead to the activation of "hidden" modes [64,65]. Let us concentrate here on the chemisorbed species, which appear as depressions in the STM images. On those molecules adsorbed close to a step edge or kink, the shape in STM images reveals a distorted adsorption geometry, probably due to the reduced symmetry of the surrounding atomic sites. On these molecules an additional peak at ± 39 meV appears in the spectra. This peak is tentatively associated with the stretching of the molecule with respect to the surface. Surprisingly, the other two peaks are not affected, remaining at the same position and with the same shape. The origin of the activation of a new vibrational signal is attributed to the perturbation of the symmetry of the electronic resonances due to the presence of a step, in such way that a specific mode with low cross-section may increase their coupling with the tunnelling states.

For a small molecule such as benzene, molecular orbitals are considerably broadened upon chemisorption, forming wide resonances. Several of these resonances have tails crossing the Fermi level, thus participating in the tunnelling transport. It is difficult to identify precisely which resonance excites which vibrational mode based on purely experimental data. However, the analysis of the distribution of inelastic signal within the molecular structure reveals the existence of several resonances with different symmetry.

Figure 7 plots the d^2I/dV_s^2 signal as a function of the energy (vertical axis) and as a function of the position along the diagonal of the molecule (horizontal axis). This bi-dimensional representation loses one spatial dimension but gains a direct view of the energy dependence of the inelastic signal. The three modes shown in Figure 6 appear here as bright features, with a spatial extent slightly smaller than the molecular structure. The two higher energy modes are centred with a bell-shaped distribution in the molecular structure. The spatial width at half maximum is 4.2 Å and 3.4 Å for the 19 mV and 39 mV peaks respectively. The distributions of the inelastic signal contrast with that of the lowest energy mode. In this case, the vibrational signal is very weak at the centre of the topographic feature, representing a value of d^2I/dV_s^2 smaller than 1%, but has stronger intensity at both sides of the molecule up to about $d^2I/dV_s^2 \sim 10\%$. The distance between both maxima is 6.4 Å and thus the maximal intensity is obtained with the tip outside the molecular ring.

The differences in the signal distribution for every mode reveal the participation of several molecular resonances in the inelastic scattering processes. As in the case of C_{60} on Ag(110) shown before, or in the previously reported work by Hann et al. [52] for O_2 on Ag(110), inelastic maps may reflect directly the shape of the resonances involved in the excitation. Free benzene orbitals are well

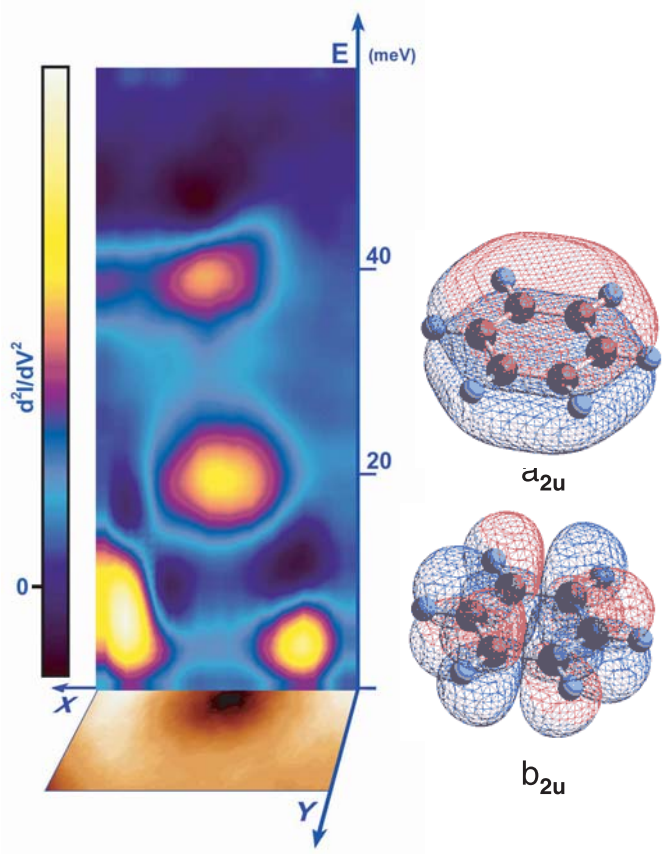

Fig. 7. Two dimensional colour scale representation of the d^2I/dV_s^2 signal as a function of the energy and the distance along one line crossing the "S" benzene molecule in Figure 6. The line is perpendicular to a [100]-oriented step edge, which is located at the left side. For clarity, in the bottom image we represent the scaled topography of the molecule ($I = 2$ nA, $V_s = 0.1$ V, $V_{ac} = 4$ mV rms at $f_{ac} = 641$ Hz). For comparison, the figure also shows the spatial shape of the two π orbitals of a free benzene molecule: the lowest orbital, a_{2u} has no nodal point at the centre. Higher lying orbitals (here shown the probably unoccupied b_{2u} orbital) present nodal planes.

known. The bell-distribution of the higher energy inelastic peaks resembles the lowest energy π state of a free benzene molecule — a_{2u}. The shape of the lowest peak resembles a resonance with a nodal point at the centre of the molecule. In general, the inelastic maps are consistent with the spatial distribution of the molecular resonances, supporting the general picture of resonant mechanism of vibrational excitation. It is also remarkable that vibrational modes which lie only 15 meV apart are activated by different electronic resonances, which are usually several eV's wide.

The nature of the coupling between vibrational and electronic states is thus behind the "selection" rules for the activation of vibrations. Besides excitation, the detection of the inelastic signal depends on the effect of a molecular vibration on the tunnelling conductance. The problem is not simple, and probably there is not a way of extracting a list of rules, but instead, detailed simulations must be produced for every adsorption system. Therefore, complementary theoretical modelling of both excitation and detection processes is important for extracting information from the experimental results.

3 Quenching of molecular vibrations through reaction coordinates

A fundamental difference between molecular reactions in gas phase and on a metal surface lies in the existence for the latter of fast quenching mechanisms mediated by substrate excitations. The metal surface provides a continuum spectrum of excitations consisting in the creation of electron-hole pairs or excitation of phonon modes. These are the dominant channel for adsorbing the energy of a molecular excitation. They also can adsorb the excess energy when additional damping channels are followed during the relaxation process. In fact, intramolecular energy transfer between vibrations or fast energy re-distribution competes with fast damping only through substrate excitations.

Experiments on single molecules have demonstrated that beyond direct excitation of modes in the reaction coordinate, the tunnel electrons may also induce a reaction by excitation of modes in a different coordinate [28–32,34]. In this case the anhamornicity of the potential energy surface allows effective coupling between modes, mediating the energy transfer between different vibrational states. The group of Ho found that excitation of internal stretching modes of O_2 and C_2H_2 induce molecular rotation [28,32]. Besides the intermode coupling the nature of the chemisorption process may affect strongly the quenching rate through a reaction pathway. For example, Komeda and co-workers found that CO diffuses on a Pd(110) surface upon excitation of internal C–O stretch, while this was not the case on Cu(110), even though the barrier for lateral diffusion is lower here [30]. In this case, the difference lies not only in the magnitude of the anharmonic coupling between excited and reaction coordinate. The authors show that, in addition to a strong coupling between internal and external modes, a lower number of excitations for climbing the activation barrier also leads to higher reaction rates [66].

These results demonstrate the role of internal reaction pathways in a regime of low power, typically nanowatts, where energy redistribution is not sufficient to induce a reaction. An advantage of using a STM is not only the accessibility to such low power regime, but the high sensitivity for detecting reaction outcomes. STM can detect reactions with quantum yields (reaction per incident electron) lower than 10^{-10}. Thus, the combination of both low power and high sensitivity makes the STM a valuable tool to study reaction mechanism at surfaces in the limit where mode specificity applies.

In order gain understanding on these internal pathways of energy transfer we investigate a model system, ammonia adsorbed on Cu(100), whose stimulated desorption induced by electrons and by photons has been amply studied [8,13,67–69]. Ammonia desorption shows an interesting intra-molecular dynamics since excitation of the umbrella mode (also called the inversion mode because it leads to inversion of the structure in the gas phase) induces the cleavage of the chemisorption bond via a conformational inversion of the molecule. This desorption mechanism was found after irradiation of UV light [67] and also after impact of ballistic electrons [68]. Photodesorption of NH_3 from a Cu(100) surface has been also stimulated by IR laser pulses, which couple resonantly with the umbrella (δ_s(N–H)) [69] or the N–H stretch (ν_s(N–H)) modes [13]. The mechanism proposed (*resonant heating* [15]) consist in the excitation of the fundamental vibrational excitation followed by quenching via multiple excitations of the reaction coordinate. The power density of these experiment was 8.5 nW/nm^2. Thus, it is the appropriate system to provide an alternative view as seen by a local and sensitive technique [31].

3.1 The experiment: mode-selective manipulation of NH_3 dynamics

Figure 8a shows an STM image of a clean Cu(100) region with three NH_3 molecules. The molecules are chemisorbed on the surface after gas-dosage at temperatures close to 5 K. At the surface, the molecules occupy the on top position with the 3-fold symmetry axis oriented perpendicular to the surface. A chemical bond is formed by the nitrogen lone pair electrons interacting directly with the metal surface. The bond is strong enough for stable STM imaging. The chemisorption well is ∼600 meV deep, as obtained after thermal desorption measurements [70] and DFT calculations [37].

However, the controlled motion of a single molecule could be reproducibly induced just by raising the sample bias voltage V_s above a certain threshold value. As a result of such procedure the molecule diffuses to a new site, just a few nanometres distant, or desorbs from the surface (Figs. 8b and 8c). Since the molecular motion implies rupture of the metal-molecule bond, we are dealing with a simple unimolecular reaction.

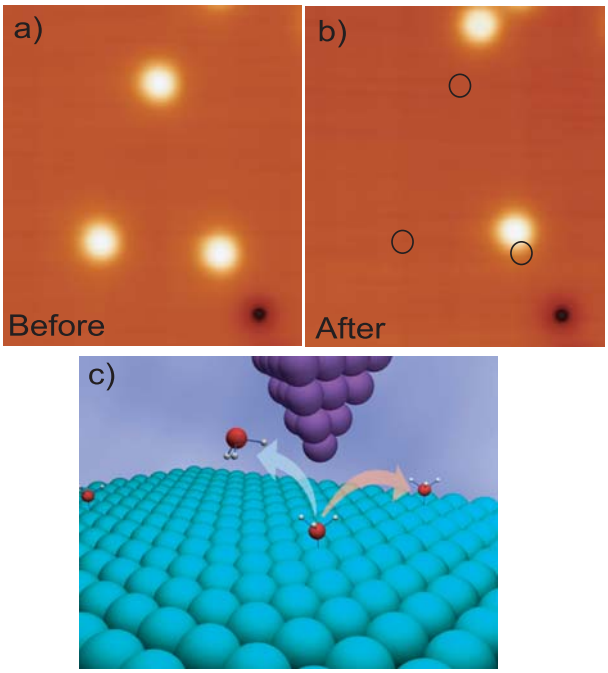

Fig. 8. (a) STM image of three NH_3 molecules before and (b) after injecting 0.5 nA of 420 meV electrons ($R \sim 1$ GΩ) on top of each molecule. Two of the molecules moved to a new site, and the third was desorbed. (c) Model of the two types of motion induced by the tunnelling electrons.

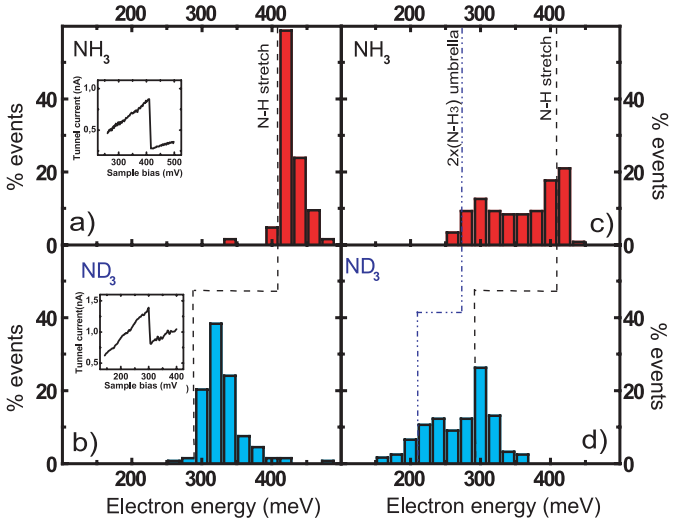

Fig. 9. Statistics of electron energy onset leading to molecular motion. Each one of the events is probed by fixing the tip above a molecule with $V_s = 100$ mV, and slowly increasing the bias voltage. A sudden current drop reveals the occurrence of a reaction. The panels show the distribution of electron energy (eV's) reached when the reaction occurs. At low tunnelling currents ($I_t < 0.5$ nA) NH_3 shows a threshold at ∼400 mV (a), which shifts down to ∼300 mV for ND_3 (b), matching correspondingly the energy of N–H and N–D stretch modes (dashed lines). These events induce molecular translation with ratio 0.6. (c) For $I_t > 1$ nA, an additional threshold appears gradually at ∼270 mV in NH_3, in consistence with the energy of two umbrella mode quanta (dash-dotted lines). Now, desorption dominates with ratio 0.75. In ND_3, the corresponding onset at ∼200 mV is observed (d) only after reaching tunnelling currents higher than 10 nA.

At this point two main analysis tools are available from the experimental side. The statistical analysis of the electron energy thresholds gives hints on the excitations activating the reaction. The dependence of the reaction yield Y_R (defined as probability per tunnelling electron) on the tunnelling current (excitation rate) resolves the number of consecutive excitation necessary for the motion.

3.1.1 Excitation of NH_3 vibrations by tunnelling electrons

Figure 9 shows the statistical distribution of the energy reached by tunnelling electrons when motion is induced. The measurements are performed by placing the STM tip on top of a molecule and slowly increasing the tunnelling bias with an open feedback loop. The tunnelling current suddenly drops when the molecule moves away from the tunnel junction (see insets in Figs. 9a and 9b). This identifies the electron energy reached when the reaction took place. The distribution of these energy values reveals a clear onset at values clearly associated with internal modes of the adsorbed NH_3. In order to confirm the vibrational assignment of the onsets, the statistics are repeated with the deuterated specie ND_3.

The results reveal the operation of two bond-breaking mechanisms, each activated by the excitation of two different internal vibrations. Reactions induced with tunnelling current smaller than 0.6 nA (Fig. 9a) show sharp energy threshold at $eV_s \sim 400$ meV due to the excitation of the N–H stretch modes, ν(N–H). This assignment is consistent with the softening of the ν(N–H) mode down to ∼300 meV found in deuterated ammonia (Fig. 9b).

When the tunnelling current during the manipulation is larger than a few nanoamperes (Fig. 9c) a second mechanism takes place. This is characterized by energy threshold at ∼270 meV, associated with the excitation of the NH_3 umbrella or inversion mode, δ_s(N–H_3), with frequency 139 meV, in coherent steps of two quanta.

DFT calculations resolve that both modes, δ_s(N–H) and ν(N–H), have the larger cross-section for inelastic scattering [37]. Upon chemisorption on a Cu(100), nitrogen $3a_1$ lone-pair electrons hybridize with Cu d-states. At the Fermi level, the density of states has a strong component derived from the original $4a_1$ LUMO states plus a small tail of the $3a_1$ (HOMO) resonance. Upon addition or removal of a $3a_1$ electron the molecule approaches a planar geometry, with very small change in the N–H bond length relative to the neutral ground state. Thus we associate the electron scattering with the $3a_1$ resonance with the excitation of the δ_s(N–H) mode. The antibonding $4a_1$ component appears largely localized at the H atoms. Thus, tunnelling through this resonance presumably produces a major effect on the N–H bond length, resulting in a more favourable excitation of the N–H stretch modes.

The case of ammonia thus gives an intuitive idea of the coupling between molecular resonances present at the Fermi level and vibrational states of the molecule. The spectroscopy experiments, however, can not resolve any mode. Calculations confirm that the inelastic fraction for this system is in the order of 10^{-3} [37]. The origin of such low excitation correction is probably related with the large separation of the highest occupied and lowest unoccupied molecular resonances respect the Fermi level, ∼5 eV and ∼2 eV respectively. It is thus interesting that, in spite of such low excitation probability, we can still probe the role of these resonances on the the reaction dynamics simply by probing the statistical distribution of the energy thresholds.

Interestingly, the reaction outcome depends on the mode used for the activation: the desorption/translation product ratio changes from 1/3, when using the N–H stretch mediated pathway, to a ratio of about 3, when the reaction is activated by the excitation of the umbrella mode. Such dependence of the reaction product on the mode excitation reveals the existence of competing pathways for the energy transfer to the reaction coordinate.

The competition between each pathway stems in different rate of accumulating energy in the reaction coordinate. For this purpose, it is important knowledge about the activation barriers to overcome. The activation barriers for molecular movement are determined by the shape of the potential energy surface (PES). For desorption, the activation energy corresponds to the ∼600 meV of chemisorption energy. Calculations of the ground state PES along the surface coordinates resolve a minimum barrier for in-plane translational of 300 meV. This lateral potential barrier corresponds to the diffusion barrier and encloses 30 bounded translational levels.

3.1.2 Dynamics of NH_3 motion

The dependence of the yield Y_R on the tunnelling current is shown in Figure 10. We determine $Y_R(eV_s, I)$ experimentally by setting fixed values of electron energy eV_s and current I_t during electron injection and accounting the average time (i.e. the average number of tunnelling electrons) employed in a reaction. The result is that for tunnelling currents in the order of 1 nA Y_R lies in the range of 10^{-10} events per electron. This value is considerably smaller than the *small* inelastic fraction of tunnelling electrons ($\sim 10^{-3}$). The difference between the two values (probability of mode excitation and probability of reaction) must lie in the parameters ruling the internal pathway for energy transference.

Independent of the complexity of specific reaction pathways, a power law dependence $Y_R \propto I_t^{n-1}$ has been found in unimolecular reactions following a ladder-climbing scheme of n vibrational excitations [71,72]. This relation justifies that in the limit of low excitation rate (excitation rate smaller than quenching rate) multi-excitation pathways are less effective as the number of excitations n becomes larger. It also predicts a non linear behavior with

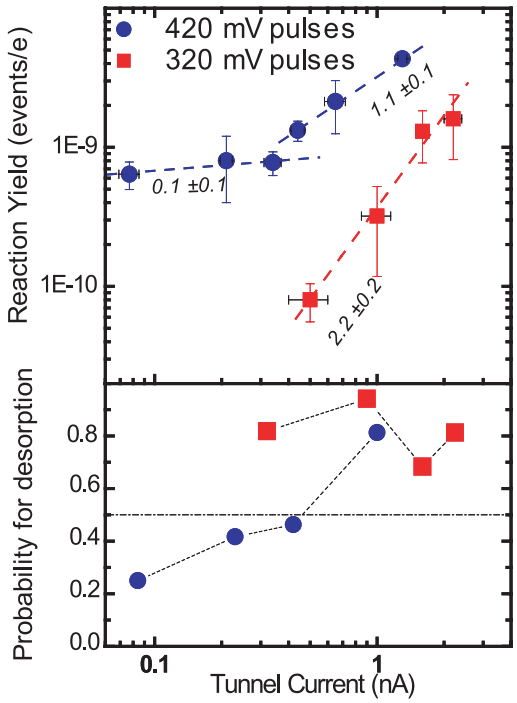

Fig. 10. Dependence of Y_R on the tunnelling current for reactions induced with 420 meV (closed circles) and 320 meV (open squares) tunnelling electrons. Lines are minimum square fits of points in each regime. Three different slopes indicate three different pathways. (Below) Desorption probability PDES as a function of tunnelling current for electron energies shown above. The probability of molecular translation is 1-PDES.

the excitation rate, from which the number of excitation can be obtained [7].

Following this analysis, the results shown in Figure 10 resolve the existence of three different pathways. Two of them are activated with electron energies above the ν(N–H) mode-frequency (eV_s = 420 meV). Here, Y_R deviates clearly from the expected power law dependence on the current. Instead, it defines two different regimes. At low tunnelling currents ($I_t < 0.5$ nA), Y_R remains essentially constant indicating a single excitation reaction mechanism. Above this threshold a mechanism described by a two-electron process becomes more favourable. The third regime is obtained when the electron energy is lowered below the onset of the ν(N–H) mode. In this case Y_R exhibits a quadratic dependence on the current, revealing a sequence of 3 vibrational excitations of the δ_s(N–H) mode.

The three distinct internal pathways of energy transfer employ a different number of excitation events and vibrational modes for the cleavage of the same bond. They manage different amounts of vibrational energy in the molecule. The single excitation pathway involves only 400 meV, so that this mode hardly can lead to molecular desorption. Instead, translation is the main product of this low current regime. On the contrary, above the 0.5 nA cross over, and for the pathway activated by the ν(N–H) mode, desorption dominates as main product.

In both cases, the energy accumulated by the multiple excitations exceeds the adsorption energy. The bond-cleavage reaction will take place whenever this energy is focused in the final coordinate.

In combination with model calculations it is possible to partially resolve the different steps taking place in every pathway [37,73]. The resulting model involves not only knowledge on the nature of the mode excited, number of excitations and activation barriers to overcome. It is also necessary to understand the coupling between modes, which is enhanced by anharmonicities of the potential and the continuum of substrate excitation which adsorbs the excess energy. The translational pathway is a clear example since the ν(N–H) mode does not actuate directly on translational coordinates.

Also, the probability for exciting a ν(N–H) mode, 8×10^{-4} excitations per electron, is much larger than the experimental yield of the translational pathway, 6×10^{-10} events per electron. Since this pathway employs a single excitation, the different between both probabilities must be due to the efficiency of energy transfer between the activated coordinate and the reaction coordinate. Theoretical modelling the N–H stretch-to-translation damping reproduces the $\sim 10^{-6}$ factor found in our experiment [37]. The importance of these decay channels illustrates how intramolecular energy transfer may become an important phenomena in surface chemistry.

When the electron flux through the molecule is large enough to overcome the decay rate of the first ν(N–H) excitation, multi-electron pathways come into effect. The result of these is the accumulation of sufficient vibrational energy in the molecule to overcome the adsorption well. In general terms, the energy accumulation will be favored in those modes having a larger excitation and lower damping rates. This is the case of the umbrella mode. In addition, the molecular inversion is able of steering molecular desorption [67,68]. Therefore, this mode plays a major role in the desorption pathway.

The three excitation pathway places energy directly into the umbrella mode. It is probable probable that two excitations invert the molecule and the third one leads to desorption. Due to the low fraction of inelastic electrons for this system, the ladder climbing sequence proceeds minimizing the number of excitations. A pathway involving 5 excitations of the δ_s(N–H_3) each in a one-step sequence, will only dominate when the tunnelling rate approaches the umbrella decay rate, as it was indeed found in the work of Bartels et al. [29].

The two electron pathway is more difficult to unravel. Rate equations describe several possibilities for this pathway (Fig. 11b), all possibly leading to energy accumulation into the inversion coordinate [73]. On the one hand, a double excited ν(N–H) state could decay into δ_s(N–H_3). On the other hand, the fundamental excitation of a ν(N–H) state can decay into the umbrella mode twice. Here, the energy is accumulated in the reaction coordinate. This mechanism is similar to a resonant heating by laser-vibration coupling in infra-red photo-desorption experiments [15].

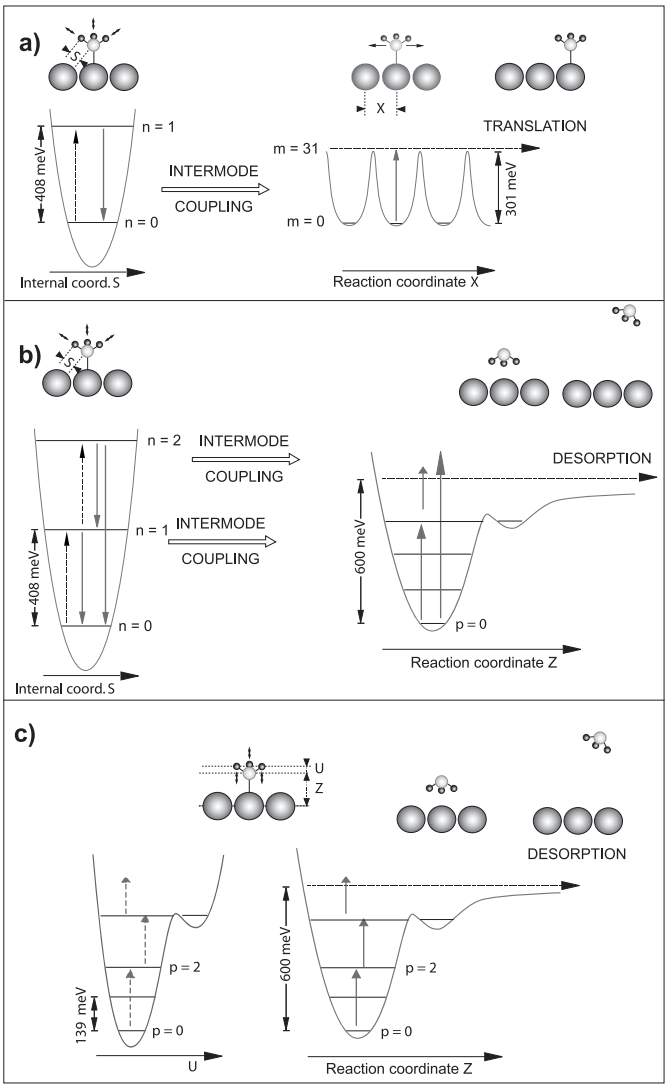

Fig. 11. Scheme and one-dimensional potentials of single, double, and triple reaction pathways leading to the cleavage of the NH_3–Cu(100) bond. (a) Single excitation: 420 meV electrons excite the N–H stretch mode (dashed arrow). Upon decay of the vibrational excitation there is a finite probability of exciting hindered translational states via anharmonic inter-mode coupling. Population of states $m \geqslant 30$ produces molecular motion above the 301 meV barrier for diffusion. (b) Double excitation: Several pathways could explain experimental results, all of them involving also the excitation of the N–H stretch coordinate, and damp into the inversion coordinate which leads to desorption. One of them follows twice the excitation fundamental internal mode, which decays accumulating the energy in the reaction coordinate. If the double excitation occurs in the internal mode, it will decay in one or two steps into umbrella modes. (c) Triple excitation: for 320 meV electrons the N–H stretch is a closed channel. Only the umbrella mode is operative. The two potential wells along the inversion coordinate (U) are no longer symmetric for the chemisorbed molecule. The inverted minimum is 360 meV above the umbrella state $p = 0$. This mode induces molecular motion along the adsorption coordinate Z, and thus, steers desorption by inverting the ammonia molecule. The possible three excitations needed to overcome the 600-meV adsorption well are drawn.

4 Summary

In summary, we present here a scheme of reactivity obtained by reviewing previous works on single molecule chemistry by STM. The manipulation mediated by tunnelling electrons is able of producing information about elementary processes, which in many cases complement the picture obtained by other spectroscopies.

Here we have concentrated on vibrational mediated chemistry, with is activated by the fast tunnelling processes via molecular resonances. The excitation of a vibration depends on the nature of electron-phonon coupling. Therefore it is not possible to extract a predefined set of selection rules, since they change with the nature of the chemisorption processes. Two model systems, fullerenes and benzene on Ag(110) has been presented here to illustrate the role of molecular resonances on the excitation.

These vibrations may provide sufficient energy to the molecule to activate a specific chemical transformation, generally being a bond cleavage. Our investigations on a model adsorbate system, NH_3 on Cu(100), reveal that the excitation of ammonium internal modes activates the rupture of the adsorption bond, leading to motion along two different coordinates. Several pathways take place and can be selected by selecting the values of tunnelling current and electron energy. In particular, we find that the selective excitation of ammonium stretching or bending modes allows control over the outcome of such bond-cleavage reaction. From our results, and based on model calculations presented elsewhere [37,73,74], we have provided a coherent picture that accounts for energy delivery processes between internal to external coordinates.

References

1. R.D. Levine, R.B. Bernstein, *Molecular Reaction Dynamics and Chemical Reactivity* (Oxford University Press, New York, 1987)
2. *Laser spectroscopy and photochemistry on metal surfaces*, edited by H.L. Dai, W.E. Ho (World Scientific, Singapore, 1995)
3. *Mode Selective Chemistry*, edited by J. Jortner, R.D. Levine, B. Pullman (Kluwer Academic Publishers, Dordrecht, 1991)
4. F.F. Crim, Science **249**, 1237 (1990)
5. F.F. Crim, Acc. Chem. Res. **32**, 877 (1999)
6. D.G. Busch, S.W. Gao, R.A. Pelak, M.F. Booth, W. Ho, Phys. Rev. Lett. **75**, 673 (1995)
7. G.P. Salam, M. Persson, R.E. Palmer, Phys. Rev. B **49**, 10655 (1994)
8. P. Saalfrank, G.K. Paramonov, J. Chem. Phys. **107**, 10723 (1997)
9. J. Higgings, A. Conjusteau, G. Scoles, S.L. Bernasek, J. Chem. Phys. **114**, 5277 (2001)
10. F.-J. Kao, D.G. Busch, D. Gomes da Costa, W. Ho, Phys. Rev. Lett. **26**, 4098 (1993)
11. G. Ertl, M. Neumann, Z. Naturforsch. Teil A **27**, 1607 (1972)
12. L.P. Levine et al., J. Appl. Phys. **38**, 331 (1967)
13. T.C. Chuang, I. Hussla, Phys. Rev. Lett. **52**, 2045 (1984)
14. I. Hussla, H. Seki, T.C. Chuang, Z.W. Gortel, H.J. Kreutzer, P. Piercy, Phys. Rev. B **32**, 3489 (1985)
15. Z.W. Gortel, H.J. Kreuzer, P. Piercy, R. Teshima, Phys. Rev. B **27**, 117 (1983)
16. D.M. Eigler, E.K. Schweizer, Nature **344**, 524 (1990)
17. M.F. Crommie, C.P. Lutz, D.M. Eigler, Science **262**, 218 (1993)
18. J. Kliewer, R. Berndt, S. Crampin, New J. Phys. **3**, 22 (2001)
19. K.F. Braun, K.H. Rieder, Phys. Rev. Lett. **88**, 096801 (2002)
20. N. Nilius, T.M. Wallis, W. Ho, Science **297**, 1853 (2002)
21. L. Bartels, G. Meyer, K.H. Rieder, Phys. Rev. Lett. **79**, 697 (1997)
22. B.C. Stipe, M.A. Rezaei, W. Ho, S. Gao, M. Persson, B.I. Lundqvist, Phys. Rev. Lett. **78**, 4410 (1997)
23. S.W. Hla, L. Bartels, G. Meyer, K.H. Rieder, Phys. Rev. Lett. **85**, 2777 (2000)
24. Y. Kim, T. Komeda, M. Kawai, Phys. Rev. Lett. **89**, 126104 (2002)
25. P. Avouris, R.E. Walkup, A.R. Rossi, H.C. Akpati, P. Nordlander, T.C. Shen, G.C. Abeln, J.W. Lyding, Surf. Sci. **363**, 368 (1996)
26. P.A. Sloan, R.E. Palmer, Nature **434**, 367 (2005)
27. D.M. Eigler, C.P. Lutz, W.E. Rudge, Nature **352**, 600 (1991)
28. B.C. Stipe, M.A. Rezaei, W. Ho, Phys. Rev. Lett. **81**, 1263 (1998)
29. L. Bartels, M. Wolf, T. Klamroth, P. Saalfrank, A. Kuhnle, G. Meyer, K.H. Rieder, Chem. Phys. Lett. **313**, 544 (1999)
30. T. Komeda, Y. Kim, M. Kawai, B.N.J. Persson, H. Ueba, Science **295**, 2055 (2002)
31. J.I. Pascual, N. Lorente, Z. Song, H. Conrad, H.P. Rust, Nature **423**, 525 (2003)
32. B.C. Stipe, M.A. Rezaei, W. Ho, Science **279**, 1907 (1998)
33. L. Bartels, G. Meyer, K.H. Rieder, D. Velic, E. Knoesel, A. Hotzel, M. Wolf, G. Ertl, Phys. Rev. Lett. **80**, 2004 (1998)
34. H. Ueba, Surf. Rev. Lett. **10**, 771 (2003)
35. R.E. Walkup, D.M. Newns, P. Avouris, Phys. Rev. B **48**, 1858 (1993)
36. N. Lorente, M. Persson, Phys. Rev. Lett. **85**, 2997 (2000)
37. N. Lorente, J.I. Pascual, Phylos. Trans. **362**, 1227 (2004)
38. J. Gaudioso, W. Ho, J. Am. Chem. Soc. **123**, 10095 (2001)
39. J. Gaudioso, W. Ho, Angew. Chem. Intern. Ed. **40**, 4080 (2001)
40. J. Gaudioso, L.J. Lauhon, W. Ho, Phys. Rev. Lett. **85**, 1918 (2000)
41. G. Binnig, G. García, H. Rohrer, Phys. Rev. B **32**, 1336 (1985)
42. B.N.J. Persson, J.E. Demuth, Solid State Commun. **57**, 769 (1986)
43. P.K. Hansma, *Tunneling Spectroscopy* (Plenum, New York, 1982)
44. R.C. Jacklevic, J. Lambe, Phys. Rev. Lett. **17**, 1139 (1966)
45. B.N.J. Persson, Baratoff, Phys. Rev. Lett. **59**, 339 (1987)
46. J.I. Pascual, N. Lorente, in *Properties of Single Molecules on Crystal Surfaces*, edited by W. Hoffer (to be published, 2005)
47. L.J. Lauhon, W. Ho, Rev. Sci. Instrum. **72**, 216 (2001)
48. B.C. Stipe, M.A. Rezaei, W. Ho, Rev. of Sci. Instrum. **70**, 137 (1999)
49. B.C. Stipe, M.A. Rezaei, W. Ho, Science **280**, 1732 (1998)
50. W. Ho, J. Chem. Phys. **117**, 11033 (2002)

51. Y. Sainoo, Y. Kim, T. Komeda, M. Kawai, J. Chem. Phys. **120**, 7249 (2004)
52. J.R. Hahn, H.J. Lee, W. Ho, Phys. Rev. Lett. **85**, 1914 (2000)
53. J.I. Pascual, J. Gomez-Herrero, C. Rogero, A.M. Baro, D. Sanchez-Portal, E. Artacho, P. Ordejon, J.M. Soler, Chem. Phys. Lett. **321**, 78 (2000)
54. D. Purdie, H. Bernhoff, B. Reihl, Surf. Sci. **364**, 279 (1996)
55. J.G. Hou, J.L. Yang, H.Q. Wang, Q.X. Li, C.G. Zeng, H. Lin, W. Bing, D.M. Chen, Q.S. Zhu, Phys. Rev. Lett. **83**, 3001 (1999)
56. H.Q. Wang, C.G. Zeng, B. Q.X. Li, J.L. Wang, J.L. Yang, J.G. Hou, Q.S. Zhu, Surf. Sci. **442**, L1024 (1999)
57. C. Rogero, J.I. Pascual, J. Gomez-Herrero, A.M. Baro, J. Chem. Phys. **116**, 832 (2002)
58. T. David et al., Phys. Rev. B **50**, 5810 (1994)
59. P. Ordejón et al., Phys. Rev. B **53**, R1041 (1996)
60. D. Sanchez Portal, P. Ordejon, E. Artacho, J.M. Soler, Int. J. Quant. Chem. **65**, 453 (1997)
61. M.S. Dresselhaus, G. Dresselhaus, P.C. Eklund, *Science of fullerenes and carbon nanotubes* (Academic Press, San Diego, 1996)
62. J.I. Pascual, J.J. Jackiw, Z. Song, P.S. Weiss, H. Conrad, H.P. Rust, Phys. Rev. Lett. **86**, 1050 (2001)
63. J.I. Pascual, J.J. Jackiw, Z. Song, P.S. Weiss, H. Conrad, H.P. Rust, Surf. Sci. **502**, 1 (2002)
64. L.J. Lauhon, W. Ho, J. Phys. Chem. A **104**, 2463 (2000)
65. T. Komeda, Y. Kim, Y. Fujita, Y. Sainoo, M. Kawai, J. Chem. Phys. **120**, 5347 (2004)
66. B.N.J. Persson, H. Ueba, Surf. Sci. **502**, 18 (2002)
67. T. Hertel, M. Wolf, G. Ertl, J. Chem. Phys. **102**, 3414 (1995)
68. A.R. Burns, D.R. Jennison, E.B. Stechel, Phys. Rev. Lett. **72**, 3895 (1994)
69. I. Hussla, T.C. Chuang, Ber. Bunsenges. Phys. Chem. **89**, 294 (1985)
70. K.J. Wu, D.V. Kevan, J. Chem. Phys. **94**, 7494 (1991)
71. J.A. Prybyla, T.F. Heinz, J.A. Misewich, M.M.T. Loy, J.H. Glownia, Phys. Rev. Lett. **64**, 1537 (1990)
72. W. Ho, Acc. Chem. Res. **31**, 567 (1998)
73. H. Ueba, T. Mii, N. Lorente, B.N.J. Persson, J. Chem. Phys. (2005, in press)
74. N. Lorente, J.I. Pascual, H. Ueba, Surf. Sci. (2005, in press)